JOURNAL OF MATERIALS SCIENCE 3 (1968) 165–173

The Effective Surface Energy of Brittle Materials

R. W. DAVIDGE, G. TAPPIN
Ceramics Division, United Kingdom Atomic Energy Authority Research Group, Atomic Energy Research Establishment, Harwell, Berks, UK

Received 1 November 1967

The effective surface energy of four brittle materials, alumina, poly(methylmethacrylate), glass, and graphite, is calculated from load/deflection curves of notched bars deformed in three-point bending. Two of the methods, which are commonly used in fracture mechanics studies, *viz* the modified Griffith treatment and the compliance analysis method, are concerned with the effective surface energy at the initiation of fracture, γ_I. The third method, the work of fracture test, is concerned with the mean effective surface energy over the whole fracture process, γ_F. The two estimates of γ_I give consistent values, and there is no systematic variation of γ_I with notch depth. Values of γ_F decrease with increasing notch depth as the fracture process becomes more controlled. For alumina $\gamma_I \sim \gamma_F$. For PMMA and glass $\gamma_I > \gamma_F$ because of a multiplicity of crack sources during fracture initiation. For graphite $\gamma_I < \gamma_F$ because of subsidiary cracking as fracture proceeds.

1. Introduction

The effective surface energy is a property of fundamental importance in determining the mechanical properties of brittle materials. It is defined here as the work done to create unit area of new fracture face, not taking into account the fine scale surface irregularities of the fracture face. For a given material the effective surface energy (γ) is not necessarily the same at all stages in the fracture process. Two values of γ are of particular interest: γ_I, pertaining to the initiation of fracture, and γ_F, the work of fracture, the value averaged over the whole fracture process.

γ_I* is simply the value of γ used in the Griffith equation, and is related to the strain energy release rate at the instant of fracture by $-(\partial U/\partial A) \geqslant \gamma_I$, where A is the area of new fracture face. $(\partial U/\partial A)$ may be obtained by theoretical or experimental methods.

γ_F is obtained by measuring the work done to completely fracture a specimen in a controlled manner [1, 2].

This paper is concerned with the determination of γ_I and γ_F for a selection of "brittle" materials: alumina, poly(methylmethacrylate), glass, and graphite. A novel feature is that two estimates of γ_I and one of γ_F are made from the same sets of load/deflection curves for notched bars deformed in bending.

2. Experimental

The following materials were used. (*a*) Alumina: $Al_2O_3 \sim 95\%$, remainder CaO and SiO_2; Al_2O_3 grain size ~ 25 μm. (*b*) Poly(methylmethacrylate), PMMA; ICI Perspex sheet. (*c*) Glass: soda-lime type. (*d*) Graphite: pile grade "A"; maximum filler grain size ~ 1 mm. (The filler grains comprise well-aligned crystallites formed into an ordered mosaic structure).

Specimens were cut in the form of 0.5 cm square section bars 4.5 cm long. Graphite specimens were 1.0 cm square, in view of the large "grain" size, and were cut with the extrusion axis parallel to the long axis of the bar. Notches were sawn at the centre of the bars to depths c, equal to multiples of one-tenth of the beam thickness. Specimens were prepared by standard machining operations and were used in as-machined or as-ground condition.

*This should be distinguished from the commonly used fracture toughness parameter G_c which defines "A" as the area of material fractured. G_c is thus equal to $2\gamma_I$.

Five to ten specimens at each notch depth were used. Bars were deformed in three-point bending with a 4 cm span, fig. 1. Load/deflection curves

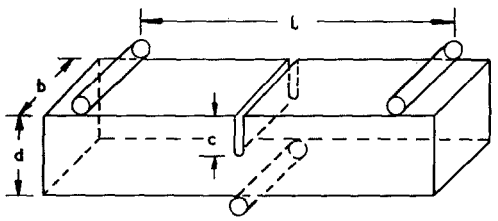

Figure 1 Specimen geometry. l = span; b = breadth; d = crack depth.

were recorded on an Instron machine operating at crosshead speeds of 0.05 to 0.005 cm/min. The machine hardness was 10^{10} dyn/cm. The fracture load and deflection and the specimen stiffness are defined in fig. 2, which shows a

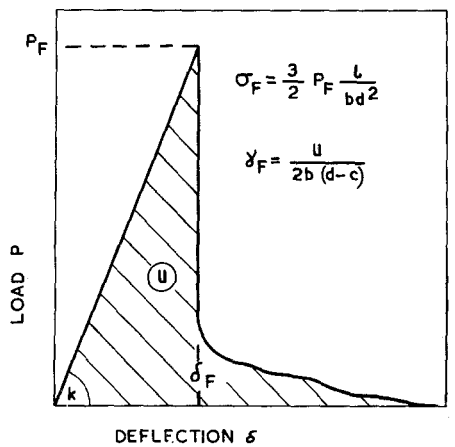

Figure 2 Load/deflection curve. P_F = fracture load; δ_F = fracture deflection; k = specimen stiffness; σ_F = fracture stress.

typical curve. The total work, U, done during the test, was recorded on an integrator.

3. Determinations of γ

3.1. Methods Based on the Initial Rate of Strain Energy Release

The strain energy release rate $(\partial U/\partial A)$ may be obtained either by an analytical method or by the experimental method of compliance analysis. The former method involves determination of $(\partial U/\partial A)$ from the mathematically computed stress distribution around the notch for the particular specimen geometry in question [3-8]. The compliance analysis method derives $(\partial U/\partial A)$ solely from experimental load/deflection curves.

3.1.1. Analytical Method

The effective surface energy determined by this method will be referred to as γ_G. When the notch depth is small compared with the beam depth, γ_G is given by [3, 4]

$$\gamma_G = -\left(\frac{\partial U}{\partial A}\right) = \frac{(1-\nu^2)\pi\sigma_F^2 c}{2E} \qquad (1)$$

where: ν is Poisson's ratio; E is Young's modulus; and σ_F is the fracture stress, $3P_F l/2bd^2$. Plain-strain conditions are assumed. Equation 1 is essentially the original Griffith equation.

When $c/d \geqslant 0.1$ approximately, corrections must be applied to this equation and various mathematical treatments are available [5, 6], many of which are reviewed by Srawley and Brown [7]. For convenience the expressions are often presented in the form

$$\gamma_G = \frac{9(1-\nu^2)\,P_F^2 l^2 \mathrm{f}(c/d)}{8Eb^2\,(d-c)^3} \qquad (2)$$

where $\mathrm{f}(c/d)$ is a dimensionless parameter. At small c/d values $\mathrm{f}(c/d) = \pi c(d-c)^3/d^4$, and equation 2 reduces to equation 1. Fig. 3 shows $\mathrm{f}(c/d)$ as a function of c/d, as calculated from results of Gross and Srawley [6] by Corum [8]. Fig. 3 strictly applies only to beams deformed in

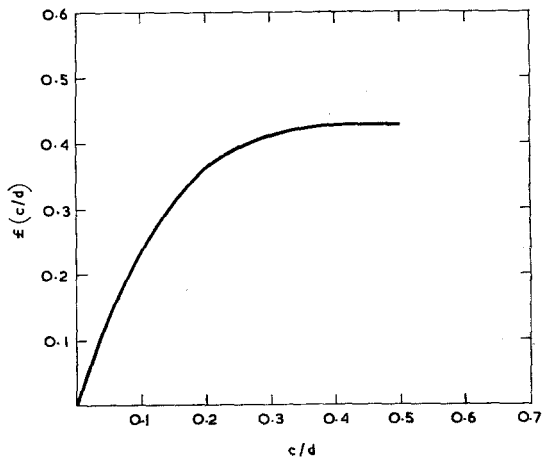

Figure 3 f(c/d) versus c/d [7, 8].

four-point bending, but provided that $l \geqslant 8b$ approximately, corrections due to the shear stresses present during three-point bending are small (<10%) [7].

The geometrical constants can be compounded with $\mathrm{f}(c/d)$ to give,

$$\gamma_G = \frac{(1-\nu^2)\,P_F^2 F}{E} \qquad (3)$$

where $F = 9l^2f(c/d)/8b^2(d-c)^3$, values of which are given in table I for $l = 4$ cm and $b = d = 0.5$ cm.

TABLE I Values of F as a function of c/d, for use in equation 3.

c/d	$f(c/d)$	$F = \frac{9\,l^2 f(c/d)}{8\,b^2(d-c)^3}$ * (cm^{-3})
0.1	0.23	182
0.2	0.36	405
0.3	0.41	690
0.4	0.43	1150
0.5	0.43	1980
0.6	0.43	3870

*$l = 4$ cm, $d = b = 0.5$ cm

3.1.2. Compliance Method

The effective surface energy determined by this method will be referred to as γ_C and this should equal γ_G. The load/deflection curve in fig. 1 is given by $P = k\delta$ so that the stored energy at the instant of fracture is $U = P_F\delta_F/2$ or $k\delta_F^2/2$.

Now, $\gamma_C = -(\partial U/\partial A)_\delta$, fracture occurring at a fixed deflection. Or, $\gamma_C = -(\partial U/\partial k)_\delta.(\partial k/\partial A)_\delta$. But $(\partial U/\partial k) = \delta_F^2/2$ and thus

$$\gamma_c = -\delta_F^2\,(\partial k/\partial A)/2. \qquad (4)$$

Experimentally one has to measure the specimen stiffness k as a function of the initial crack area, $A = 2bc$. For each notch depth used, $(\partial k/\partial A)$ is obtained from the slope of the curve at the appropriate value of A, as in fig. 4. Substitution

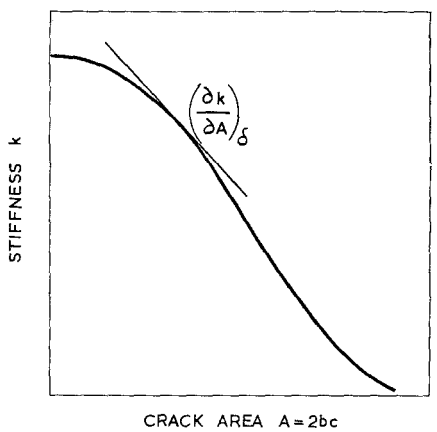

Figure 4 General form of k versus A curve.

of these values of $(\partial k/\partial A)$ in equation 4 with the experimental values for δ_F thus gives a series of γ_C values for each notch depth.

3.2. Work of Fracture Method [1, 2]

Most brittle materials fracture catastrophically when deformed in three-point bending. However, when a sufficiently deep notch is present the specimen is so much weakened that the total stored energy becomes small compared with the surface energy required to break the specimen; in this case controlled fracture follows as in fig. 2. Energy is also stored in the testing machine and it is thus advantageous to use as hard a machine as possible. The work of fracture is given simply by

$$\gamma_F = \frac{U}{2b(d-c)} \qquad (5)$$

4. Results

A representative set of load/deflection curves, for PMMA, is given in fig. 5. Un-notched bars

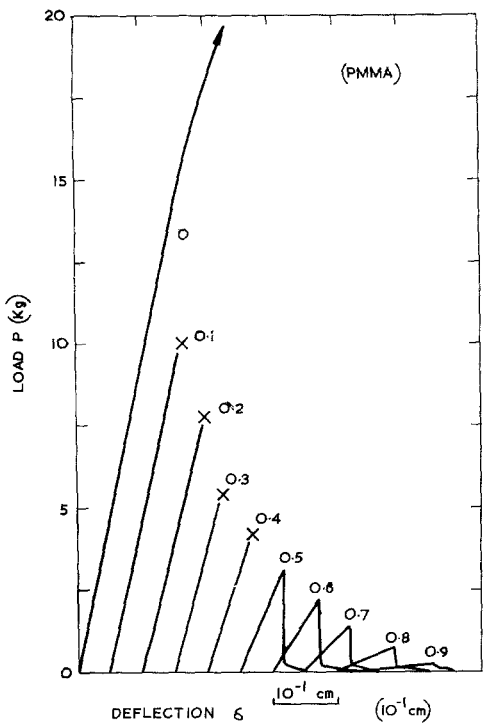

Figure 5 Load/deflection curves for PMMA. Numbers on graph refer to notch depth ratio c/d. X indicates catastrophic failure.

exhibited extensive viscous flow and no estimate of the fracture load was obtained. Only specimens with $c/d \geqslant 0.5$ showed controlled fracture. All the alumina and glass samples behaved in an essentially elastic manner up to fracture with

controlled crack growths, similar to PMMA, for $c/d \geqslant 0.2$ and 0.5 respectively. All the graphite specimens showed controlled crack growth with irregular load/deflection curves once fracture was initiated, fig. 6.

Data for all specimens of the four materials are summarised in table II. Each result is the mean value for five to ten specimens at each notch depth. Figs. 7 to 10 are plots of k versus A, from which values of $-(\partial k/\partial A)$ were obtained. Young's moduli were determined from the stiffness of the un-notched bars using the formula $E = kl^3/4bd^3$. Elastic properties are summarised as table III.

TABLE II Summary of data for calculation of γ_C,γ_G, and γ_F.

Material	c/d	P_F	k	δ_F	$-(\partial k/\partial A)$	$\gamma_C = -\partial_{P_F^2}$ $(\partial k/\partial A)/2$	$\gamma_G = P_F^2 F(1-\nu^2)/E$	γ_F
		(10^6 dyn)	(10^9 dyn/cm)	(10^{-3} cm)	(10^{10} dyn/cm^3)	(10^4 erg/cm^2)	(10^4 erg/cm^2)	(10^4 erg/cm^2)
Alumina	0.0	60.1	12.3	4.90	—	—	—	—
	0.1	23.1	13.2	1.75	—	—	2.7	—
	0.2	16.1	11.3	1.42	3.52	3.6	3.0	6.6
	0.3	12.6	9.5	1.33	4.36	3.8	3.1	5.6
	0.4	9.8	6.95	1.41	4.50	4.5	3.2	5.3
	0.5	7.1	4.97	1.43	3.44	3.5	2.8	5.1
	0.6	5.3	3.64	1.46	3.08	3.3	3.1	4.9
	0.7	3.3	1.90	1.74	2.54	3.8	—	4.6
	0.8	1.8	0.99	1.82	1.65	2.7	—	4.4
	0.9	0.59	0.25	2.36	1.03	2.9	—	3.8
		(10^6 dyn)	(10^7 dyn/cm)	(10^{-1} cm)	(10^8 dyn/cm^3)	(10^5 erg/cm^2)	(10^5 erg/cm^2)	(10^5 erg/cm^2)
PMMA	0.0	—	11.96	—	—	—	—	—
	0.1	10.36	11.45	0.90	1.56	6.4	5.6	—
	0.2	7.69	10.45	0.73	2.24	6.1	7.0	—
	0.3	5.57	9.20	0.60	2.82	5.2	6.2	—
	0.4	4.33	7.51	0.58	3.50	5.9	6.2	—
	0.5	3.21	5.79	0.55	3.50	5.4	5.9	3.6
	0.6	2.41	3.83	0.63	3.38	6.7	6.5	3.4
	0.7	1.46	2.33	0.63	2.68	5.3	—	3.2
	0.8	0.72	1.10	0.65	2.09	4.5	—	2.8
	0.9	0.26	0.26	1.00	0.95	4.7	—	3.0
		(10^6 dyn)	(10^9 dyn/cm)	(10^{-3} cm)	(10^9 dyn/cm^3)	(10^3 erg/cm^2)	(10^3 erg/cm^2)	(10^3 erg/cm^2)
Glass	0.0	17.7	2.78	6.37	—	—	—	—
	0.1	5.14	2.61	1.97	5.7	11.0	6.4	—
	0.2	3.60	2.26	1.60	7.0	9.0	7.0	—
	0.3	2.66	1.75	1.52	7.2	8.3	6.5	—
	0.4	2.13	1.43	1.49	7.2	8.0	7.0	—
	0.5	1.72	1.19	1.45	7.2	7.6	7.9	6.8
	0.6	1.18	0.81	1.46	7.2	7.7	7.2	5.4
	0.7	0.84	0.46	1.83	5.8	9.7	—	5.6
	0.8	0.43	0.21	2.05	4.3	9.0	—	5.0
		(10^6 dyn)	(10^9 dyn/cm)	(10^{-3} cm)	(10^9 dyn/cm^3)	(10^4 erg/cm^2)	—	(10^4 erg/cm^2)
Graphite	0.0	38.4	2.18	17.6	—	—	—	22.7
	0.1	25.0	2.13	11.7	—	—	—	14.0
	0.2	20.3	2.08	9.7	0.47	2.2	—	14.0
	0.3	16.0	1.96	8.2	1.14	3.8	—	15.1
	0.4	13.3	1.61	8.3	2.15	7.4	—	13.7
	0.5	8.82	1.09	8.1	2.33	7.7	—	13.2
	0.6	5.81	0.68	8.6	1.73	6.4	—	11.1
	0.7	3.53	0.396	8.9	1.28	5.1	—	11.9
	0.8	1.66	0.162	10.2	0.93	4.7	—	10.6
	0.9	0.43	0.025	17.2	—	—	—	8.4

Effective surface energies, γ_G, γ_C and γ_F using equations 3, 4 and 5, are plotted, as a function of c/d for the four materials, in figs. 11 to 14. No γ_G values are quoted for graphite because the specimen geometry was unsuitable.

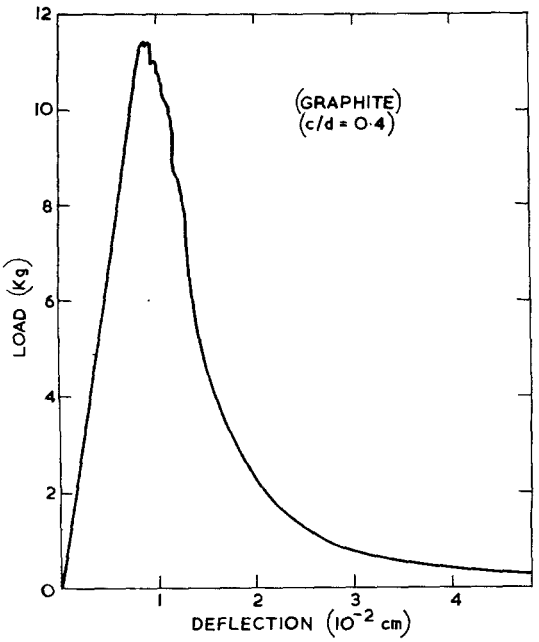

Figure 6 Controlled load/deflection curve for graphite.

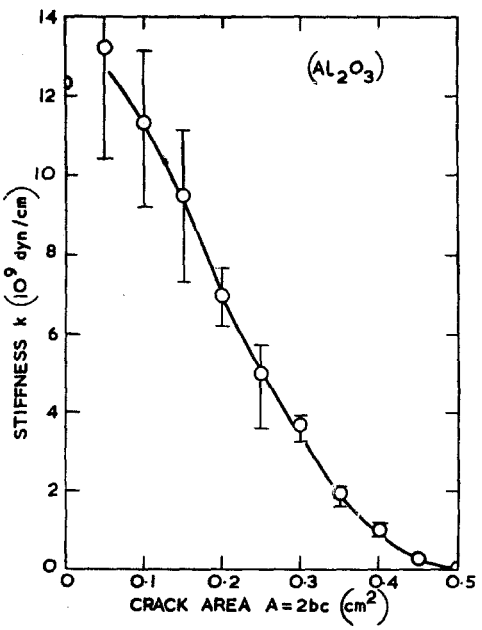

Figure 7 k versus *A* data for alumina.

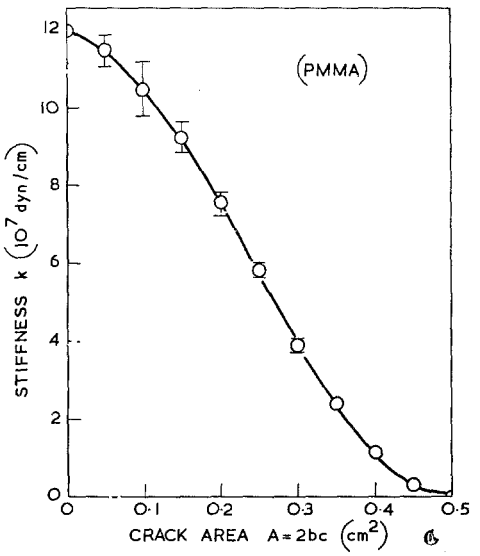

Figure 8 k versus *A* data for PMMA.

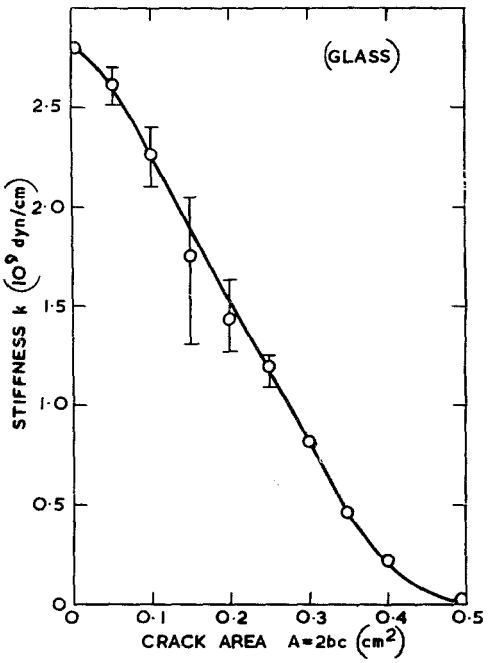

Figure 9 k versus *A* data for glass.

TABLE III Elastic constants for the four materials.

Material	Young's Modulus (dyn/cm²)	Poisson's Ratio
Al_2O_3	3.20×10^{12}	0.3
PMMA	3.08×10^{10}	0.33
glass	7.10×10^{11}	0.21
graphite	3.49×10^{10}	0.11

5. Discussion

The effective surface energies of four brittle materials have been measured by three independent methods. Two methods involve the surface energy at the instant of fracture; the third involves the average surface energy over the total fracture process. The methods will be discussed first, and then the results for each material in turn.

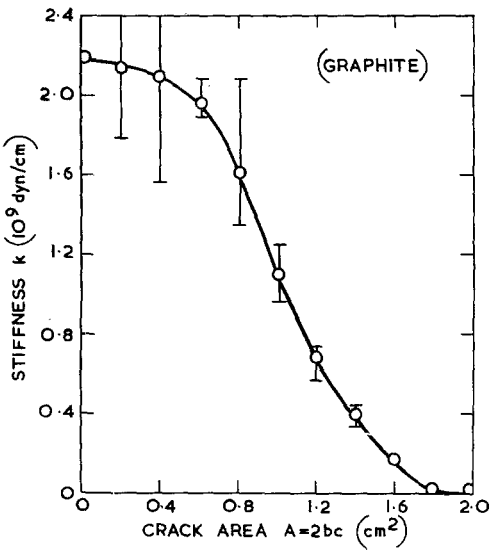

Figure 10 k versus A data for graphite.

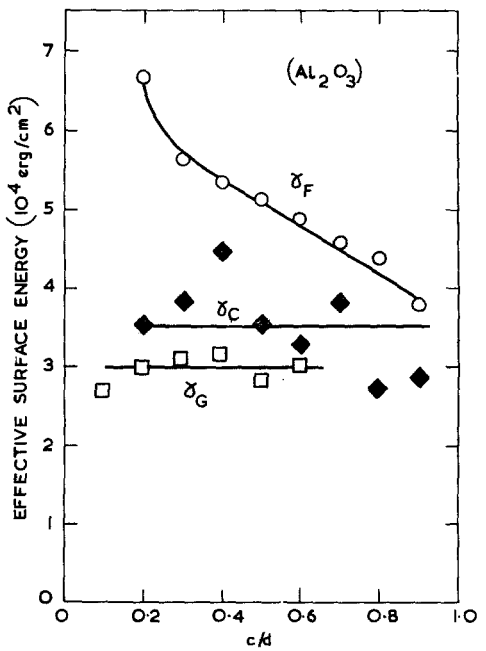

Figure 11 Values of γ_G, γ_C, and γ_F for alumina.

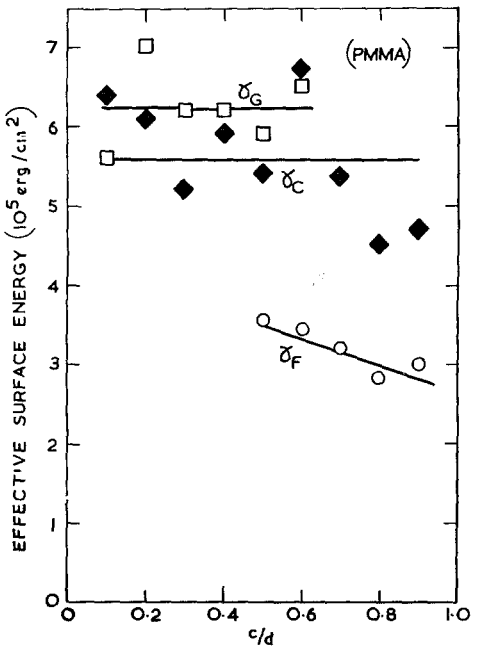

Figure 12 Values of γ_G, γ_C, and γ_F for PMMA.

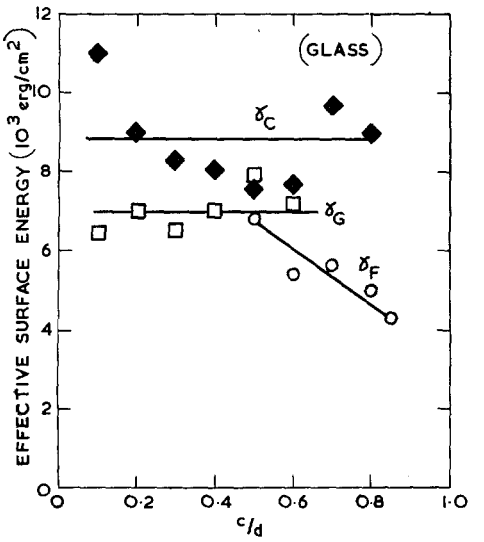

Figure 13 Values of γ_G, γ_C, and γ_F for glass.

5.1. Methods for Determination of γ

The analytical and compliance methods for the determination of γ_I show good agreement. There is no systematic variation of either γ_G or γ_C as a function of c/d and both γ_G and γ_C show a scatter of up to $\pm 20\%$ from the mean value. The mean values of γ_G and γ_C for a particular material are within 10 to 20% of each other.

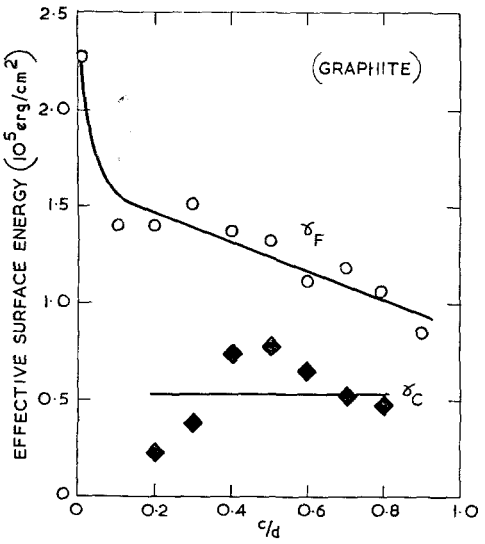

Figure 14 Values of γ_C and γ_F for graphite.

These γ_I values were determined from the strain energy release rates at the instant of fracture initiation. It has not been established that γ_I is a material property alone. Indeed, it will be shown below that γ_I values are very dependent on the precise testing procedure, in particular on the initial distribution of crack sources. The γ_I values quoted here are thus strictly relevant only to specimens prepared and tested as above.

Results for the work of fracture γ_F do show a trend as a function of c/d, γ_F decreasing with increasing notch depth. This behaviour is general for all four materials and in graphite, which exhibits stable cracks at all notch depths, γ_F varies by a factor of 2.5. This effect has been associated with increasing control of crack growth (i.e. decreasing crack velocity) with increasing notch depth [2]. Chances of energy loss will be greatest when the crack velocity is highest and the specimen possesses kinetic energy. A second possibility is that energy losses will be greatest when the material is under high stress. Specimens with small notches will have a larger proportion of material under high stress than specimens with large notches and thus a higher probability of energy loss. Both these effects suggest that the γ_F values obtained for deep notch depths will be closest to the true effective surface energy.

Granted that the true γ_F value is given by extrapolating results to $c/d = 1$, the relative values of γ_F and γ_I show three types of behaviour: $\gamma_F = \gamma_I$ for alumina; $\gamma_F < \gamma_I$ for PMMA and glass; and $\gamma_F > \gamma_I$ for graphite. This implies that the energies absorbed in crack initiation and crack propagation are unequal for each of the three latter materials.

5.2. Results for Individual Materials

5.2.1. Alumina

γ_I and γ_F values are within the range quoted for similar materials [1]. Substitution of $\gamma_G = \gamma_I = 3.2 \times 10^4$ erg/cm^2 into equation 1 gives a critical flaw size for the un-notched bars of ~ 80 μm, this is about three grain diameters. It should be possible to detect such flaws prior to fracture. However, the flaws are not necessarily present in the as-machined material and may form under the combined action of applied stresses below the fracture stress and internal stresses [9, 10]. These cracks can grow at grain or phase boundaries with an energy absorption rate of $\sim 10^3$ erg/cm^2. Macroscopic fracture follows only when conditions are such as to satisfy the higher value of γ_I of 3.2×10^4 erg/cm^2.

5.2.2. PMMA and Glass

Both PMMA and glass have $\gamma_I > \gamma_F$. Since, furthermore, PMMA exhibits a "glass-like" fracture, it is convenient to discuss these materials together. Previously quoted values of γ_I lie in the ranges 1 to 5×10^5 erg/cm^2 for PMMA [11-13] and 3 to 10×10^3 erg/cm^2 for glass [2, 14]. These are more in accordance with the present values for γ_F than for γ_I. The reason for this apparently high value of γ_I lies in the crack configuration at the root of the notch.

Examination of fracture faces shows three distinct regions: a zone of severe hackle, extending ~ 50 μm below the notch, where fracture has originated from numerous sources along the root of the notch; an intermediate zone where several approximately parallel cracks, connected by tongue-like configurations, have extended $\leqslant 500$ μm approximately; and finally the normal mirror-like fracture. Fig. 15 is an example for glass.* The tongues represent the disturbed region where two parallel non-coplanar cracks interact and overlap. In materials like glass that do not show a preferred crystallographic cleavage plane the two cracks associated with

*A similar effect has been observed in single-crystal alumina. This could explain the surprisingly high values for the surface energy of sapphire obtained by J. Congleton and N. J. Petch [*Acta Met.* **14** (1966) 1179].

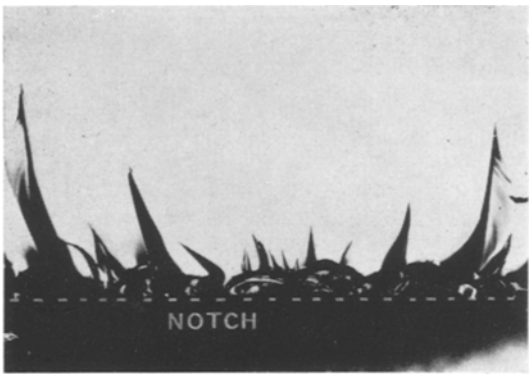

Figure 15 Fracture face of fractured glass specimen (reflected light, ×85).

the tongue coalesce as fracture proceeds; this is in contrast to materials like MgO where the two cracks remain parallel and displaced [15].

The present γ_I results are thus concerned with multiple crack initiation and tongue formation. The γ_F results, however, are related primarily to the mirror-like fracture since they relate to the total fracture process. It is easily demonstrated that the energy absorption rate during multiple crack initiation is greater than that during mirror-like fracture. Single sharp cracks were introduced into PMMA specimens with a razor blade to $c/d \sim 0.5$, so that subsequent fracture was mirror-like. In this case the fracture deflection, δ_F, was $\sim 70\%$ of the corresponding value for standard notched bars. Since from equation 4 γ_I is proportional to δ_F^2, the γ_I value for mirror-like crack initiation is about one-half of the value for multiple crack initiation. Good agreement between γ_I and γ_F can therefore be expected only when they refer to the same mode of fracture.

Substitution of $\gamma_G = \gamma_I = 7 \times 10^3$ erg/cm^2 in equation 1 gives for un-notched glass bars a critical crack size of 46 μm. (The parallel calculation for PMMA is not possible because un-notched bars fractured only after considerable viscous flow). Cracks thus grow through the region of severe hackle before catastrophic failure occurs. This initial growth of microcracks presumably proceeds via a stress corrosion process so that only a low surface energy is required. A recent discussion of these effects is reported by Wiederhorn [16].

5.2.3. Graphite

For graphite, crack initiation requires less energy than crack propagation. Corum [8] has measured γ_I for a similar graphite (EGCR-type AGOT) and obtains a value of 3×10^4 erg/cm^2 (cf 5×10^4 erg/cm^2); he reports no value for γ_F but a rough estimate may be made from his load/deflection curves, and $\gamma_F \sim 2 \times 10^5$ erg/cm^2 (cf 1×10^5 erg/cm^2). The reason for the high energy absorption during crack growth must lie in the tortuous crack path, and the secondary cracks that open up during fracture [17].

The value of $\gamma_G = 5 \times 10^4$ erg/cm^2 when substituted in equation 1 with current data gives a critical flaw size of 0.2 mm.

6. Conclusions

(i) The analytical and compliance methods for estimating the effective surface energy for crack initiation γ_I give similar and consistent values for notched beams deformed in bending.

(ii) Work of fracture values decrease with increasing notch depth due to various energy dissipative processes that are more relevant at shallow notch depths. The values obtained at large notch depths are considered to be more reliable.

(iii) Good agreement between γ_I and γ_F is expected only when fracture initiation and fracture propagation processes are similar. Such agreement cannot be assumed and must be investigated for each material and set of experimental conditions.

(iv) For materials undergoing a glass-like fracture, crack initiation is more difficult than crack propagation because of a multiplicity of surface crack sources. A material containing many small crack sources may therefore be more resistant to catastrophic failure than a material containing few sources.

(v) Materials containing many volume crack sources, as graphite, show a greater resistance to crack propagation than to crack initiation.

Acknowledgements

Thanks are due to Dr F. J. P. Clarke and Dr G. D. Miles for numerous stimulating discussions, and to Dr J. Williams for his support of this programme.

References

1. H. G. TATTERSALL and G. TAPPIN, *J. Matls. Sci.* **1** (1966) 296.
2. J. NAKAYAMA, *J. Amer. Ceram. Soc.* **48** (1965) 583.
3. G. R. IRWIN, *Trans. ASM* **40A** (1948) 147.
4. E. OROWAN, *Welding J.* **34** (1955) 157.

5. D. H. WINNE and B. M. WUNDT, *Trans. ASME* **80** (1958) 1643.
6. B. GROSS and J. E. SRAWLEY, NASA Report TN-2603, 1965.
7. J. E. SRAWLEY and W. F. BROWN, "Fracture Toughness Testing and its Application" (ASTM, 1964) and NASA TM X-52030 (1964).
8. J. M. CORUM, USAEC Report ORNL-4030 (1966).
9. F. J. P. CLARKE, *Acta Met.* **12** (1964) 139.
10. R. W. DAVIDGE and G. TAPPIN, *J. Matls. Sci.* **3** (1968) to be published.
11. J. J. BENBOW and F. C. ROESLER, *Proc. Phys. Soc.* **B70** (1957) 201.
12. J. P. BERRY, *J. Appl. Phys.* **34** (1963) 62.
13. A. VAN DEN BOOGAART, "Physical Basis of Yield and Fracture" (Phys. Soc., London, 1966) p. 167.
14. E. B. SHAND, *J. Amer. Ceram. Soc.* **44** (1961) 21.
15. F. F. LANGE and K. A. D. LAMBE, *Phil. Mag.* in press.
16. S. M. WIEDERHORN, *J. Amer. Ceram. Soc.* **50** (1967) 407.
17. R. H. KNIBBS, *J. Nucl. Matls.* **24** (1967) 174.